

Geometry-Based Next Frame Prediction from Monocular Video

Reza Mahjourian^{1,2*} Martin Wicke² Anelia Angelova²

Abstract—We propose a method for next frame prediction from video input. A convolutional recurrent neural network is trained to predict depth from monocular video input, which, along with the current video image and the camera trajectory, can then be used to compute the next frame. Unlike prior next-frame prediction approaches, we take advantage of the scene geometry and use the predicted depth for generating next frame prediction. A useful side effect of our technique is that it produces depth from video, which can be used in other applications.

We evaluate the proposed approach on the KITTI raw dataset, which is collected from a vehicle moving through urban environments. The results are compared with the state-of-the-art models for next frame prediction. We show that our method produces visually and numerically superior results to existing methods that directly predict the next frame.

I. INTRODUCTION

Scene understanding, *i.e.*, attaching meaning to images or video, is a problem with many potential applications in computer vision, computer graphics, and robotics. We are interested in a particular test for such approaches: whether they are able to predict what happens next, *i.e.*, given a video stream, predict the next frame in the video sequence.

Traditionally, many such approaches have been model-based, with strong assumptions about what kind of scenes are permissible [18], [10] *e.g.*, a bouncing ball or a rigid object. Such assumptions lead to a parametric model of the world, which can be fitted to the observations. For example, assuming that a camera observes only one object, one can conceivably fit the degrees of freedom of the object and their rates of change to best match the observations. Then, one can use generative computer graphics to predict the next frame to be observed. While model-based methods [18], [10] perform well in restricted environments, they are not suitable for unconstrained environments.

On the other hand, model-free approaches do not rely on any assumption about the world and predict future frames simply based on the video stream. The simplest such techniques use a 2D optical flow field computed from the video to warp the last frame [24]. The resulting next frame prediction is not optimized for visual quality, but work well in applications such as video compression. Recent methods based on neural networks [20], [17], [19], [21], [8] train a recurrent neural network (RNN) to predict the next frame directly from the video stream.

*This work was done at Google Brain.

¹Department of Computer Science, University of Texas at Austin, Austin, TX 78712, USA reza@cs.utexas.edu

²Google Brain, Mountain View, CA 94043, USA
wicke@google.com, anelia@google.com

Our approach is inherently model-based, however, it produces one of the most general models possible: a depth map for the scene. This type of model has the advantage that it does not impose any assumptions on the scene and therefore does not limit its generality. To achieve that we have a model-free component by training an RNN consisting of convolutional LSTM units. These units have the ability to take into account not only the current frame, but a history of video frames of theoretically unbounded length.

Contrary to prior approaches [17], [19], [21], [21], [8], we use the RNN to predict not the next video frame, but the depth map of the next video frame. Similar to classic model-based approaches, we then use generative computer graphics to render the next video frame using our predicted depth map, the current video frame, and the camera trajectory (see Figures 1 and 2). We show that this yields better outcomes in terms of visual quality, as well as, quantitative metrics, namely Peak Signal to Noise Ratio (PSNR) and the Structural Similarity Index Measure (SSIM) [14]. We are not aware of other approaches that use depth for next frame predictions.

While the depth data is needed for training the model, it is not required at serving time. The camera trajectory can be obtained from inertial measurements and gyroscopes (best), from GPS (good for large-scale motions like boats or planes), from optical flow (probably lowest quality but always available), or from analyzing a low-resolution depth camera (which does not have to be calibrated to the camera itself, just affixed to it). It is also possible to train a model to predict the near-future trajectory of the camera given its trajectory up to the current point in time, or directly from the video stream. The most suitable source for the camera trajectory depends on the hardware and situation. But its quality would impact the quality of our results.

We evaluate our approach on the KITTI raw dataset [11]. The dataset includes stereo video, 3D point clouds for each frame, and the vehicle trajectory. We only use monocular video, and show that we can extract a depth stream from the monocular video and predict the next video frame with high accuracy.

While we compare our approach with state-of-the-art models for next frame prediction, our approach has the side effect of producing depth from video. This is useful in applications such as robot navigation and planning, actuator control, and object recognition and tracking.

The main contributions of this work are:

- We propose a recurrent neural network architecture to predict depth from a sequence of monocular video frames. The network uses convolutional LSTM units to capture the motion of objects and the background. Based

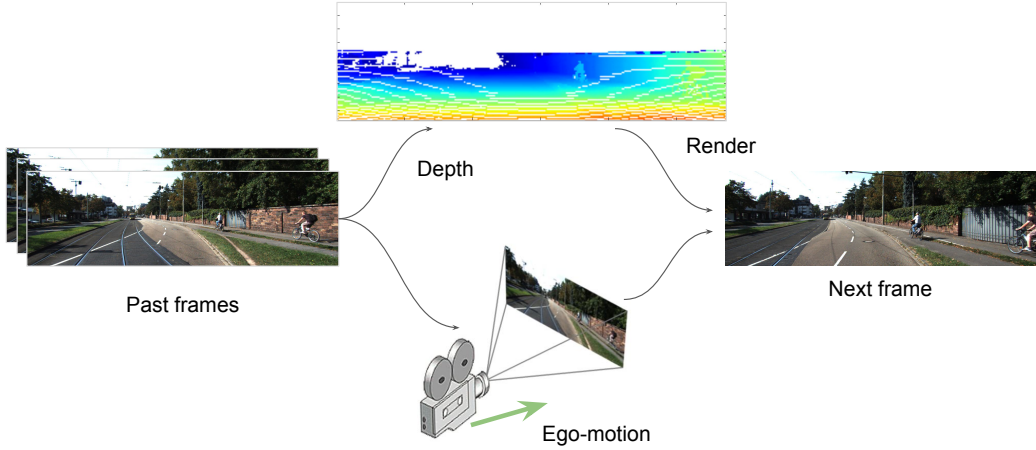


Fig. 1. Overview of the proposed method: A convolutional recurrent neural network is trained to predict depth from monocular video input, which, along with the current video image and the camera trajectory, can then be used to compute the next frame.

on the motion patterns for different regions in the source image, the network can produce a better estimate on the scene depth. Our experimental results show that seeing more input frames improves depth predictions.

- Our method creates an internal 3D model of the scene from the raw monocular video input. This 3D representation is more suitable for predicting the motion of the objects and the changes in view as a result of the viewer's own motion (ego-motion).
- We propose a model for generating next frame predictions using depth predictions and the camera's trajectory. Next frame predictions are constructed using geometric projections, translations, and rotations, which are implemented as additional network layers on top of the depth prediction output. This allows the model to directly output next frame predictions.
- The proposed method can be used to generate hypothetical next frame predictions as a result of exploratory or hypothetical actions. This capability allows a decision-making algorithm to use the next frame predictions to evaluate the potential outcomes of a set of available actions.

II. RELATED WORK

Depth Prediction from Single Images. A few methods [3], [2], [6], [16] have demonstrated the possibility of learning depth from single images using deep neural networks. The pioneering work in [3] uses a multi-scale setup to predict depth at multiple resolutions. Their model uses the lower-resolution predictions as coarse starting points for finer predictions. It also uses fully-connected layers. The state-of-the-art work in [16] uses a ResNet [12] model to improve the quality of depth predictions. We are not aware of any prior work on learning depth from a sequence of video frames, as is done in our method.

Next Frame Prediction. Unsupervised learning from large unlabeled video datasets has been a topic of recent interest [22], [23], [20], [17]. Next frame prediction using recurrent neural networks has also been proposed in [20], [17],

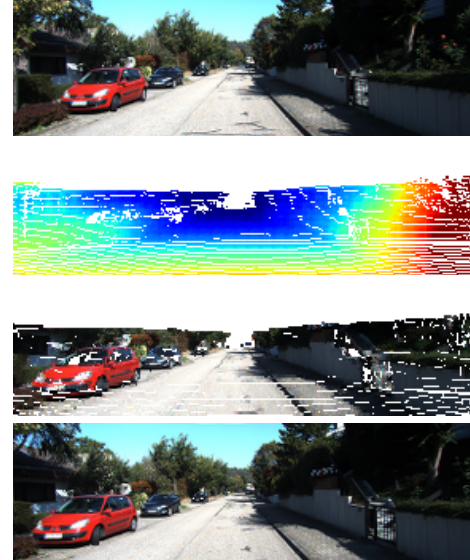


Fig. 2. Sample prediction produced by our method. From top to bottom: 1) Ground truth frame. 2) Depth prediction. 3) Next frame prediction. 4) Ground truth next frame.

[19], [25], [8]. These methods typically use a loss function based on the RGB values of the pixels in the predicted image. This results in conservative and blurry predictions where the pixel values are close to the target values, but rarely identical to them. These models usually predict a weighted average of potential outcomes. In contrast, our proposed method produces images whose RGB distribution is very close to the target next frame. Such an output is more suitable for detecting anomalies or surprising outcomes where the predicted next frame does not match the future state.

Visual State Prediction for Reinforcement Learning. Reinforcement Learning (RL) has been experiencing renewed interest with recent successes in game environments [4]. Being able to generate hypothetical next frames as a result of the agent's actions is useful in RL, especially in methods that use a state value approximator as part of their

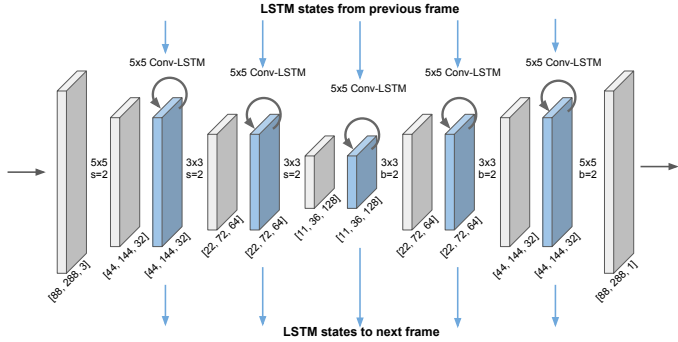


Fig. 3. The depth prediction RNN using convolutional LSTM cells. The model receives a sequence of RGB images, each with size $88 \times 288 \times 3$. It produces depth predictions of size $88 \times 288 \times 1$. The encoder uses convolutions with stride two to downsize the feature maps. The decoder uses depth-to-space layers with block size two followed by convolutions with stride one to upsize the feature maps.

policy. Most RL applications are developed for simulated environments [19] and transferring the methods to real-world environments has been difficult. Recent work [21] uses an adversarial learning approach for next frame generation in real-world environments, generating future frames with minor modifications. Our approach produces much more realistic next frames resulting from many possible hypothetical movements by the agent.

III. NEXT FRAME PREDICTION METHOD

A. Problem Formulation

The problem that our proposed method addresses can be defined as follows. Given a sequence of RGB frames $\{X_1, X_2, \dots, X_{k-1}\}$, and a sequence of camera poses $\{P_1, P_2, \dots, P_k\}$, predict the next RGB frame X_k .

B. Approach

Our proposed method predicts two depth maps D_{k-1} and D_k corresponding to frames $k-1$ and k . The depth map D_{k-1} is predicted directly from the sequence of images $X_1 \dots X_{k-1}$. The depth map D_k is constructed from D_{k-1} and the camera's ego-motion from P_{k-1} to P_k .

The next frame prediction X_k is constructed from the RGB frame X_{k-1} and the two depth maps D_{k-1}, D_k using geometric projections and transformations.

C. Depth Prediction from Monocular Video

Figure 3 shows the recurrent neural network that is used for predicting depth from monocular video. The model uses convolutions with stride two without any max-pooling layers for downsizing the feature maps in the encoder. Unlike tasks like object classification, the features in this domain are not invariant to translation. So, we avoid using max-pooling layers to preserve the spatial structure of the feature maps. In the decoder, the feature maps are gradually upsized to reach the input resolution. Upsizing is done using depth-to-space layers, which spatially rearrange the activations, followed by convolutions. The model uses convolutional LSTM cells at various spatial resolutions. Convolutional LSTM cells are

TABLE I
DEPTH PREDICTION MODEL ARCHITECTURE

Layer	Layer type and parameters	Activation size
Input	Input image	$88 \times 288 \times 3$
conv1	Conv. $5 \times 5 \times 32$ stride 2	$44 \times 144 \times 32$
ln1-1	Layer normalization	$44 \times 144 \times 32$
conv-lstm1	Conv-LSTM $5 \times 5 \times 32$	$44 \times 144 \times 32$
ln1-2	Layer normalization	$44 \times 144 \times 32$
conv2	Conv. $3 \times 3 \times 64$ stride 2	$22 \times 72 \times 64$
ln2-1	Layer normalization	$22 \times 72 \times 64$
conv-lstm2	Conv-LSTM $5 \times 5 \times 64$	$22 \times 72 \times 64$
ln2-2	Layer normalization	$22 \times 72 \times 64$
conv3	Conv. $3 \times 3 \times 128$ stride 2	$11 \times 36 \times 128$
ln3-1	Layer normalization	$11 \times 36 \times 128$
conv-lstm3	Conv-LSTM $5 \times 5 \times 128$	$11 \times 36 \times 128$
ln3-2	Layer normalization	$11 \times 36 \times 128$
ds1	Depth-to-Space block size 2	$22 \times 72 \times 32$
conv4	Conv. $3 \times 3 \times 64$ stride 1	$22 \times 72 \times 64$
ln4-1	Layer normalization	$22 \times 72 \times 64$
conv-lstm4	Conv-LSTM $5 \times 5 \times 64$	$22 \times 72 \times 64$
ln4-2	Layer normalization	$22 \times 72 \times 64$
ds2	Depth-to-Space block size 2	$44 \times 144 \times 16$
conv5	Conv. $3 \times 3 \times 32$ stride 1	$44 \times 144 \times 32$
ln5-1	Layer normalization	$44 \times 144 \times 32$
conv-lstm5	Conv-LSTM $5 \times 5 \times 32$	$44 \times 144 \times 32$
ln5-2	Layer normalization	$44 \times 144 \times 32$
ds3	Depth-to-Space block size 2	$88 \times 288 \times 8$
conv6	Conv. $5 \times 5 \times 1$ stride 1	$88 \times 288 \times 1$
sigmoid	Sigmoid	$88 \times 288 \times 1$

similar to regular LSTM cells [13], however, their gates are implemented by convolutions instead of fully-connected layers [7].

Figure 4 shows the depth prediction model unrolled through time. At each timestep, the network receives one video frame and produces one depth prediction. Since the LSTM states are retained between subsequent frames, they enable the model to capture motion between two or more frames. The output of the LSTM cells are passed to the next layer, while their states are passed through time to the next frame. Therefore, the block processing frame i receives the input frame X_i and the LSTM states S_{i-1} as inputs, where S_i is the set of LSTM states from all layers after processing frame i , and $S_0 = 0$. Unrolling the model simplifies training. Although multiple copies of the RNN are instantiated, there is a single set of model parameters shared across the instances.

Our model applies layer normalization [1] after each convolution or LSTM cell. In recurrent networks layer normalization performs better than batch normalization. Table I lists the architectural details on the depth prediction model.

We also experimented with more elaborate models, whose performance was not better than our model: 1) Adding skip connections from the encoder to the decoder. A skip connection concatenates the output of a layer in the decoder to the inputs of its corresponding similarly-sized layer in the decoder. 2) Producing and consuming intermediate low-resolution predictions as done in FlowNet [9]. The intermediate predictions were used in the loss function as well. 3) Adding a fully-connected layer plus dropout in the model bottleneck. Using a fully-connected layer resulted in overfitting.

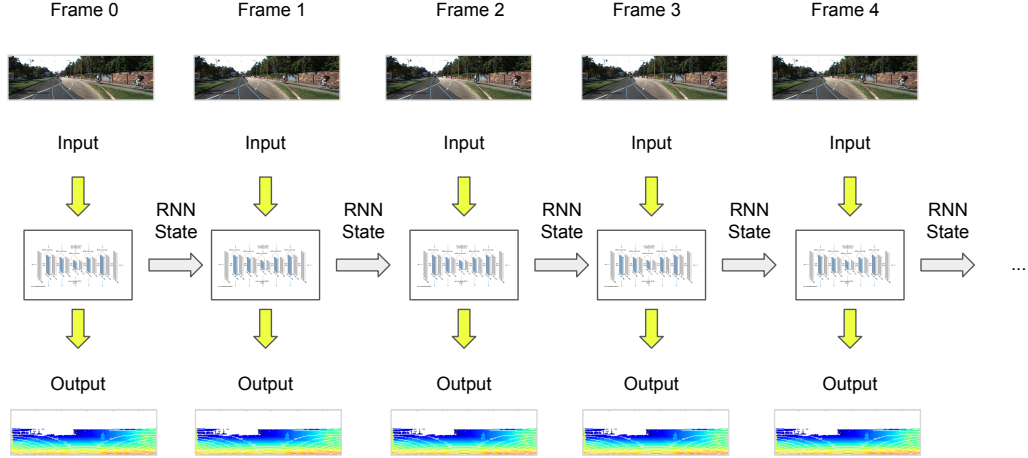


Fig. 4. Depth prediction model unrolled through time. At each timestep, the RNN receives one video frame and produces one depth prediction. The states for the LSTM cells are updated at each timestep and the updated values are used for depth prediction on subsequent frames. The output of the LSTM cells are passed to the next layer, while their states are passed through time to the next frame.

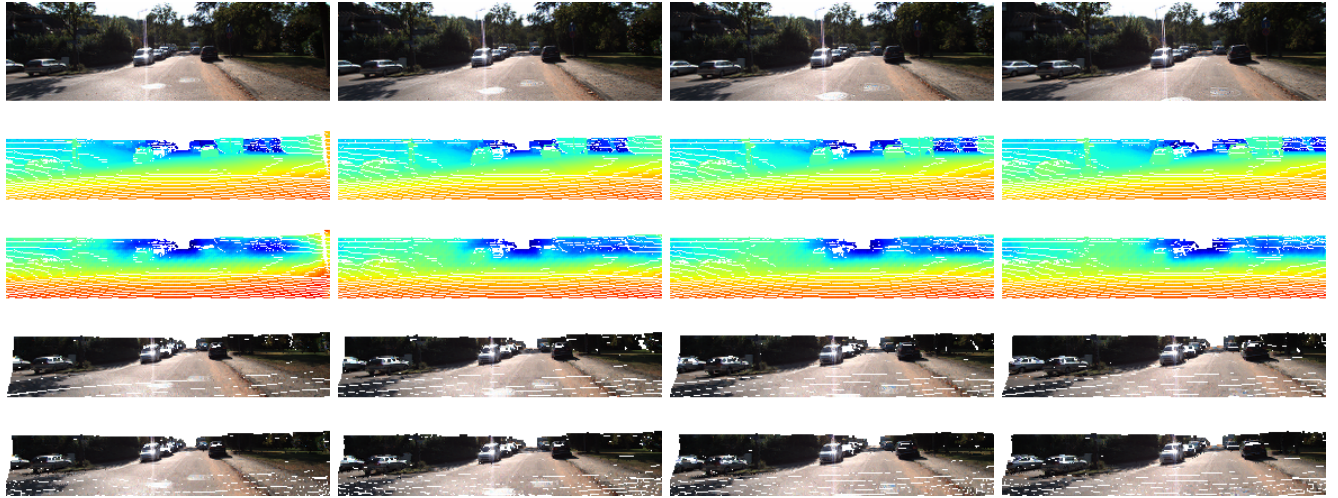


Fig. 5. Example depth and next frame predictions by our model from a four-frame sequence. The four columns show the ground truth and predictions for frames 1-4. From top to bottom in each column: 1) Ground truth frame. 2) Ground truth depth 3) Predicted depth. 4) Next frame prediction constructed using ground truth depth 5) Next frame prediction constructed using predicted depth. For frames 1-3 the ground truth next frame is visible at the top of the corresponding next column. It can be seen that the quality of depth and next frame predictions slightly improves as the model receives more video frames. After seeing only the first frame, the model believes that the ground is closer than what it actually is (visualized by a stronger red hue.) After seeing more frames, the depth estimate is improved.

D. Depth Prediction Loss Function

We experimented with the \mathcal{L}_2 and reverse Huber losses.

The \mathcal{L}_2 loss minimizes the squared euclidean norm between predicted depth D_i and ground truth depth label Y_i for frame i : $\mathcal{L}_2(D_i - Y_i) = \|D_i - Y_i\|_2^2$.

The reverse Huber loss is defined in [16] as:

$$\mathcal{B}(\delta) = \begin{cases} |\delta| & |\delta| \leq c, \\ \frac{\delta^2 + c^2}{2c} & |\delta| > c \end{cases} \quad (1)$$

where $\delta = D_i - Y_i$ and $c = \frac{1}{5} \max_i (D_i^j - Y_i^j)$ where j iterates over all pixels in the depth map. The reverse Huber loss computes the \mathcal{L}_1 norm when $|\delta| \leq c$ and the \mathcal{L}_2 norm otherwise.

Additionally, the loss equation can include an optional term to minimize the depth Gradient Difference Loss (GDL) [3], which is defined as:

$$\text{GDL}(D_i, Y_i) = \sum_{x,y} |(D_i^{x,y} - D_i^{x-1,y}) - (Y_i^{x,y} - Y_i^{x-1,y})|^2 + |(D_i^{x,y} - D_i^{x,y-1}) - (Y_i^{x,y} - Y_i^{x,y-1})|^2 \quad (2)$$

where x, y iterate over pixel rows and columns in the depth map. The purpose of the GDL term is to encourage local structural similarity between predicted and ground truth depth.

The final loss function is formed by computing the average loss over all frames in a sequence:

$$L(\theta) = \frac{1}{k} \sum_{i=1}^k \alpha_i L_\theta(D_i, Y_i) \quad (3)$$

where θ represents all model parameters, k is the number of frames in sequence, α_i is the scaling coefficient for frame i , and $L_\theta(D_i, Y_i)$ is equal to either $\mathcal{L}_2(D_i - Y_i) + \lambda_{\text{gdl}} \text{GDL}(D_i, Y_i)$ or $\mathcal{B}(D_i - Y_i) + \lambda_{\text{gdl}} \text{GDL}(D_i, Y_i)$. In experiments we set $\alpha_i = 1$ for all i , and set λ_{gdl} to either zero or one. In all loss terms, we mask out pixels where there is no ground truth depth.

E. Next Frame Prediction

The next frame prediction is generated by additional transformation layers that are added after the depth output layer (not shown in figure 4). For each frame i , the next frame prediction X'_i is generated using:

- Video frame X_{i-1} from the last timestep.
- Depth map prediction D_{i-1} from the last timestep.
- Camera poses P_{i-1}, P_i .

First, the points in depth map D_{i-1} are projected into a three-dimensional point cloud C . The x, y, z coordinates of the projected points in C depend on their two-dimensional coordinates on the depth map D_{i-1} as well as their depth values. In addition to the three-dimensional coordinates, each point in C is also assigned an RGB value. The RGB value for each point is determined by its corresponding image pixel in X_{i-1} located at the same image coordinates as the point's origin on depth map D_{i-1} .

Next, the camera's ego-motion between frames $i-1$ and i are computed from pose vectors P_{i-1} and P_i . The computed ego-motion is six-dimensional and contains three translation components t_x, t_y, t_z and three rotation components r_x, r_y, r_z . Given the camera's new coordinates and principal axis, the point cloud C is projected back onto a plane at a fixed distance from the camera and orthogonal to its principal axis. Each projected point receives an updated depth value based on its newly-calculated distance to the projection plane. The result of this projection is a depth map prediction D_i for frame i . Painting the projected points with their affixed RGB values creates the next frame prediction X'_i . Embedding the matrix multiplications that represent the necessary projections and transformations in the model allows it to directly produce next frame predictions.

The net effect of the two projections and the intermediate translation and rotation is to move pixels in X_{i-1} to updated coordinates in the predicted image X'_i . The magnitude and direction of the movement for each pixel is a function of 1) the depth of the pixel's corresponding point in the depth maps, and 2) the magnitude and direction of ego-motion components.

Since different pixels may move by different amounts, this process can produce overlapping pixels as well as gaps where no pixel moves to a given coordinate in the next frame prediction. The overlaps are resolved by picking the point whose depth value is smaller (closer to the camera). In our implementation the gaps are partly filled using a simple

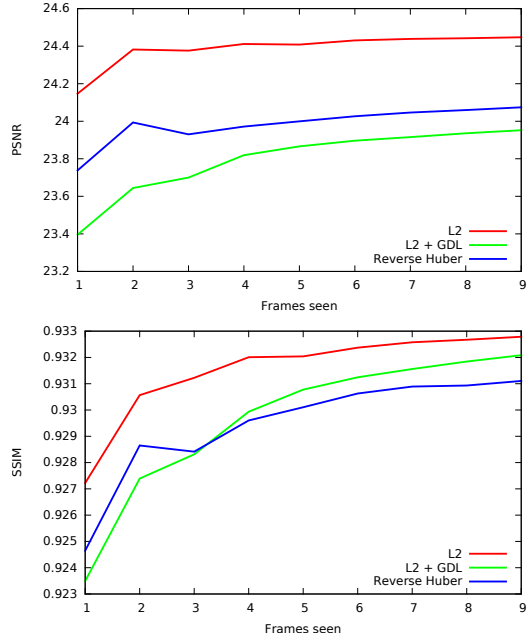


Fig. 6. Next frame prediction quality metrics as a function of the number of frames seen. The plot shows PSNR and SSIM metrics for different loss functions. For all loss functions, our RNN model performs better as it receives more video frames. The biggest jump in quality happens between frames one and two, since at that point motion information becomes available to the model. PSNR improves moderately thereafter, whereas SSIM continues to improve as more video frames are used.

splatting technique which writes each point over all four image pixels that it touches.

IV. EXPERIMENTAL EVALUATION

We test our approach on the KITTI dataset [11] which is collected from a vehicle moving through urban environments. The vehicle is equipped with cameras, lidar, GPS, and inertial sensors. The dataset is organized as a series of videos with frame counts ranging from about 100 to a few thousands. For each frame, the dataset contains RGB images, 3D point clouds, and the vehicle's pose as latitude, longitude, elevation, and yaw, pitch, roll angles.

We split the videos into training and evaluation sets and generate 10-frame sequences from each video. In total, our dataset contains about 38000 training sequences and 4200 validation sequences.

A. Generating Ground Truth Depth Maps

We generate ground truth depth maps by first transforming the point clouds using the calibration matrices in the KITTI dataset and then projecting the points onto a plane at a fixed distance from the camera. The points that are included in the depth map have depth values ranging from 3m (approximate cutoff for points visible by camera) to 80m (sensor's maximum range.) Instead of requiring the model to predict such large values, we use $(3.0 / \text{depth})$ as labels. We also experimented with using $\log(\text{depth})$ as labels. Additionally, the labels are linearly scaled to values in the interval $[0.25, 0.75]$. This normalization helps reduce the

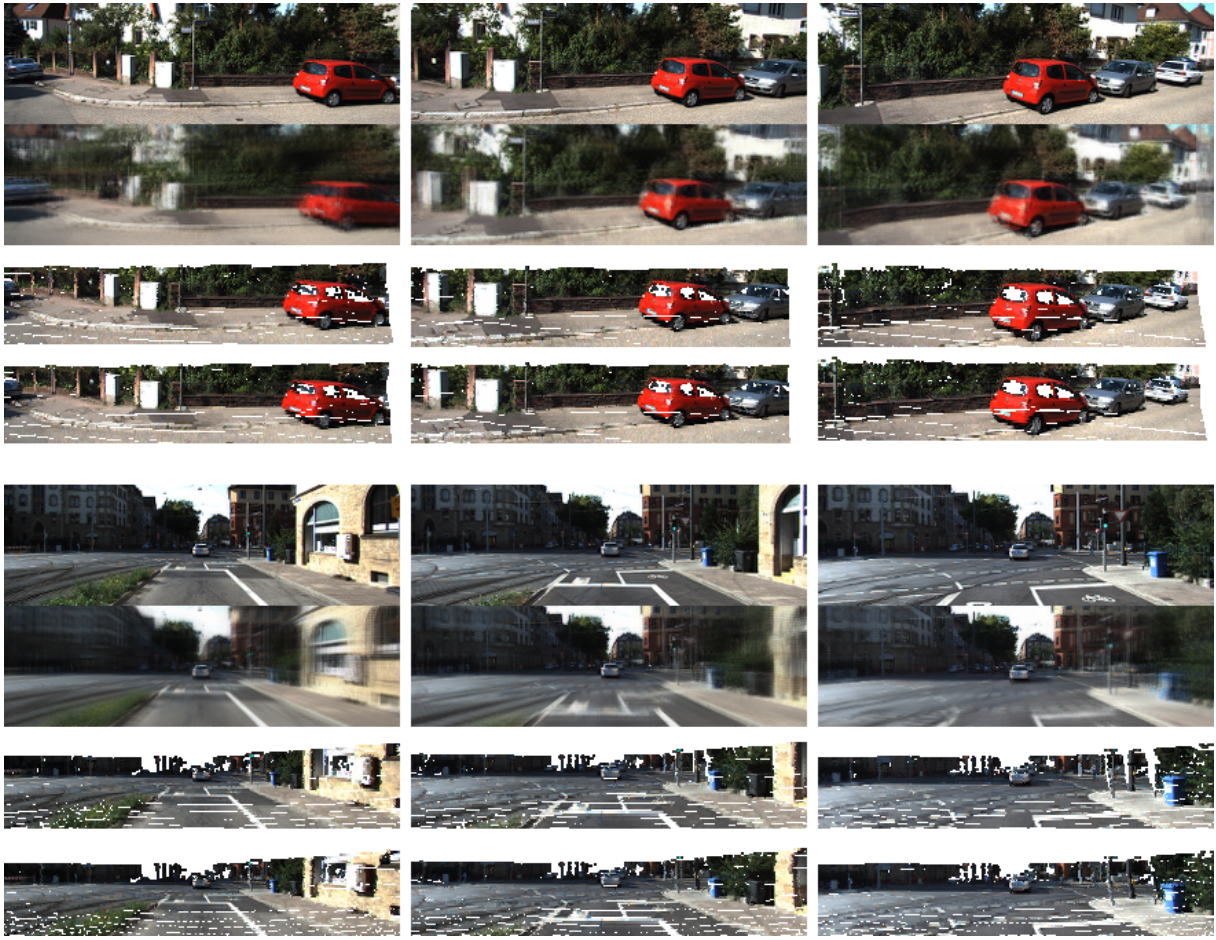


Fig. 7. Comparison of next frame prediction by our method with state-of-the-art video prediction model STP [8]. The frames shown are from the first sequence in two validation videos. In total six ground truth frames from the two videos are shown. From top to bottom in each column: 1) Ground truth last frame. 2) Prediction by STP. 3) Next frame prediction using ground truth depth. 4) Next frame prediction using predicted depth by our method. While the STP model can predict the location of objects well, it produces blurry images, especially when there is motion in the background.

imbalance between the importance of accurate predictions for points that are far and near. Without normalization, loss terms like \mathcal{L}_2 can give disproportionate weights to near and far points.

The generated depth maps contain areas with missing depth due to a number of causes: 1) Since the camera and the lidar are at different locations on the car, there are often overlaps and shadows when the point cloud is viewed from the camera. 2) Objects that are farther than the sensor's range (80m) and objects that do not reflect the light back to the sensor (shiny objects) are not detected by the sensor. 3) Since the point clouds are sparse, there are image coordinates that usually do not line up with any point.

B. Quality Metrics

We employ two image quality metrics [14] to evaluate next frame predictions produced by the model:

- Peak signal-to-noise ratio (PSNR)
- Structural similarity (SSIM)

Both metrics are standard in measuring the quality of image predictions [19], [17], [8]. Using these metrics allows us to measure the quality of predictions independently of

the loss functions and depth transform functions used. The metrics are computed for pixels where the model makes a prediction.

C. Training

Our model is implemented in TensorFlow [5]. We use the Adam optimizer [15] with a learning rate of 0.0001. The model weights are initialized from a Gaussian distribution with a standard deviation of 0.01. The LSTM states are initialized to 0.0 and the forget gates are initialized to 1.0. Each training timestep processed a mini-batch of eight 10-frame sequences. We use the \mathcal{L}_2 loss for training.

D. Results

Figure 5 shows the outputs generated by our trained model. The figure shows depth predictions and next frame predictions from four frames of a sequence. Each column corresponds to one frame. The first row shows the ground truth last frame and the last row shows next frame predictions generated using predicted depth.

By comparing the quality of depth predictions for each frame it can be observed that the model's predictions are

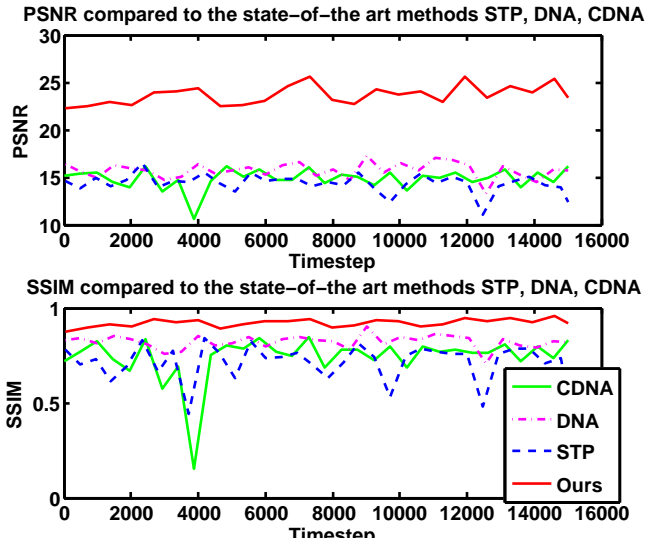


Fig. 8. Comparison of quality metrics on next frame predictions by our model against STP, DNA, and CDNA methods [8] over the validation dataset (higher values are better for both metrics). Our model clearly outperforms the previous ones in both metrics. For our model, the metrics are computed on areas where the model produces predictions. The fluctuations are partly due to the relatively small sample sizes used in the evaluation process, which we ran on CPU alongside the training process running on GPU. Each point represents an average over 72 next frame predictions from eight random sequences.

improving with seeing more frames. After seeing only the first frame, the model believes that the ground is closer than what it actually is. This is reflected in the predicted depth map as the strong red hue. By receiving more input images, the model’s depth prediction improves and turns more similar to ground truth.

This observation is also supported quantitatively in Figure 6, which shows how the quality metrics improve as a function of the number of prior frames seen by the model. The plot shows per-frame PSNR and SSIM averages over 100 mini-batches for different loss functions. As seen, for all loss functions and both metrics, the model performs better as it receives more video frames. The biggest jump in quality occurs between frames one and two, when the model gains access to the motion information in the sequence. However, the metrics continue to improve with more frames.

We further compare our next frame predictions using predicted depth, to predictions generated when using ground truth depth. The last two rows in Figure 5 show a comparison in visual quality. Figure 11 (shown later) plots the quality difference between these two sets of predictions using SSIM and PSNR metrics. These plots show that our model’s predictions track closely the best predictions possible that are based on known depth.

E. Comparison to Prior Work

To compare our model with state-of-the-art video prediction models, we trained three model variants DNA, CDNA, and STP [8] on our dataset. All the above-mentioned models are action-conditioned *i.e.*, they have placeholders to receive

state and action inputs. In addition to the video images, we pass the current camera pose as the state and the computed ego-motion as the action to all three models.

Figure 7 qualitatively compares the next frame predictions generated by our model and by the prior method of Finn et al [8]. As we can see, [8] is usually able to place the objects at the right location in the next frame. However, it produces fuzzy predictions, especially when the scene background is moving between frames. Our method, on the other hand, produces sharp and accurate predictions.

Figure 8 quantitatively compares the predictions generated by our model with DNA, CDNA, and STP. The predictions by our method outperform prior models on both PSNR and SSIM metrics. In terms of PSNR, our model performs much better by producing results in the order of 24-25, whereas the three prior methods from [8] produce values in range 15-17. Similarly for SSIM, with a maximum possible value of 1.0, our model achieves 0.92-0.93, whereas for prior methods the value is around 0.7-0.8.

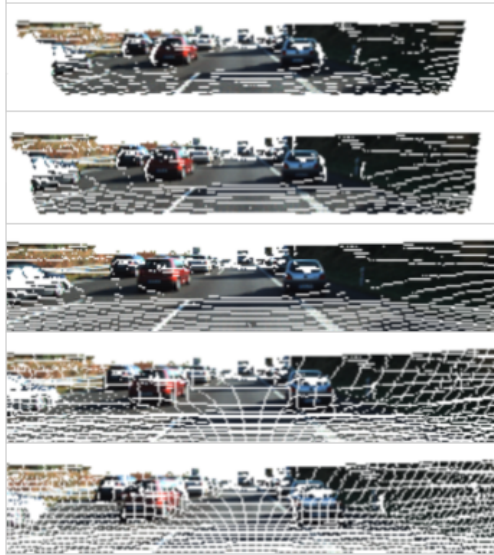


Fig. 9. Next frame simulations using ground truth depth and hypothetical ego-motions. Middle row: current frame. Other rows: Simulated next frames for moving forward/backward.

F. Failure cases

We have observed cases where the depth of thin elongated objects *e.g.*, poles are not estimated correctly. The left-most frame in Figure 5 shows an example. Since our approach is based on depth estimation, this affects the quality of our next frame predictions. The primary reason behind these errors is probably the low impact of these objects in the loss equation. Another contributing factor is the imperfect alignment of depth maps and video frames in the training data, which affects thin objects more. These misalignments are primarily due to varying time delays between the rotating lidar and the camera for different regions of the image.

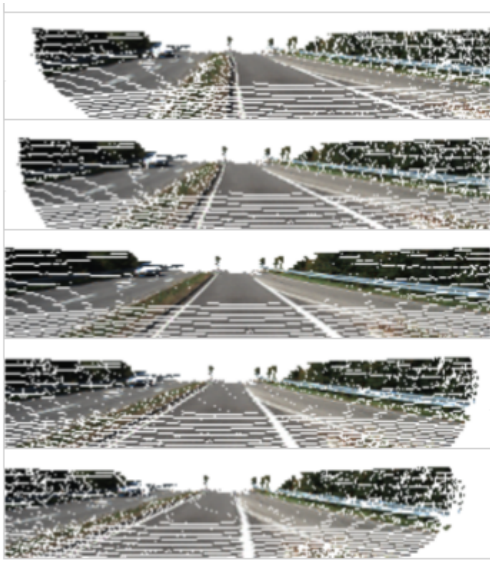


Fig. 10. Next frame simulations using ground truth depth and hypothetical ego-motions. Middle row: current frame. Other rows: Simulated next frames for moving sideways.

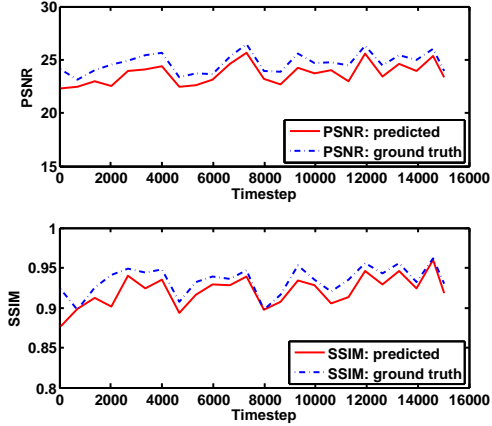


Fig. 11. Comparing quality of next frame prediction from our method using predicted depth vs next frame predictions using ground truth depth. Top: PSNR. Bottom: SSIM. Metrics are measured over small samples as training progresses. Both SSIM and PSNR are closely tracking the best predictions possible under our method.

G. Simulating Hypothetical Next Frames

Our approach can be used to generate potential next frames based on hypothetical motions of a moving agent e.g. a vehicle or a pedestrian. Such next frame simulations can be useful for exploring counterfactual world representations and for exploring the outcome of available actions in planning. Figures 9, 10 show example next frame simulations based on a range of hypothetical ego-motions corresponding to moving forward/backward and sideways. The frames shown are generated using ground truth depth. These results are best viewed as an animation. Please see the accompanying video.

V. CONCLUSIONS AND FUTURE WORK

We have presented a method for predicting the next frame from monocular video. Our method uses an RNN that is trained to predict depth from a sequence of images. Our

experiments show that the RNN can capture the motion between subsequent frames and improve its depth predictions.

We would like to improve the visual quality of the predictions by 1) upsampling and inpainting ground truth depth maps 2) inpainting next frame predictions where possible. Furthermore, predicting multiple frames into the future is a useful extension to this work. Applying our approach to anomaly detection will be an important next step. For example, we can superimpose our next frame prediction with the actually observed frame and analyze the mismatches in the scene topology (depth) or appearance (RGB frame). Large mismatches may be an indication of an object moving with an unexpected velocity, and can be used as informing signals for safer navigation.

REFERENCES

- [1] J. Ba, J. Kiros, and G. Hinton. Layer normalization. *arXiv:1607.06450*, 2016.
- [2] W. Chen, Z. Fu, D. Yang, and J. Deng. Single-image depth perception in the wild. *arXiv:1604.03901*, 2016.
- [3] D. Eigen and R. Fergus. Predicting depth, surface normals and semantic labels with a common multi-scale convolutional architecture. In *ICCV*, 2015.
- [4] D. Silver et al. Mastering the game of go with deep neural networks and tree search. *Nature*, 2016.
- [5] M. Abadi et al. Tensorflow: A system for large-scale machine learning. *arXiv:1605.08695*, 2016.
- [6] P. Wang et al. Towards unified depth and semantic prediction from a single image. In *CVPR*, 2015.
- [7] X. Shi et al. Convolutional lstm network: A machine learning approach for precipitation nowcasting. *NIPS*, 2015.
- [8] C. Finn, I. Goodfellow, and S. Levine. Unsupervised learning for physical interaction through video prediction. *NIPS*, 2016.
- [9] P. Fischer, A. Dosovitskiy, E. Ilg, P. Häusser, C. Hazırbaş, V. Golkov, P. van der Smagt, D. Cremers, and T. Brox. Flownet: Learning optical flow with convolutional networks. *arXiv:1504.06852*, 2015.
- [10] K. Fragkiadaki, P. Agrawal, S. Levine, and J. Malik. Learning predictive visual models of physics for playing billiards. *ICLR*, 2016.
- [11] A. Geiger, P. Lenz, C. Stiller, and R. Urtasun. Vision meets robotics: The kitti dataset. *IJRR*, 2013.
- [12] K. He, X. Zhang, S. Ren, and J. Sun. Deep residual learning for image recognition. *CVPR*, 2016.
- [13] S. Hochreiter and J. Schmidhuber. Long short-temp memory. *Neural Computation*, 1997.
- [14] A. Hore and D. Ziou. Image quality metrics: Psnr vs. ssim. In *Int. Conf. on Pattern Recognition*, 2010.
- [15] D. Kingma and J. Ba. Adam: A method for stochastic optimization. *arXiv:1412.6980*, 2014.
- [16] I. Laina, C. Rupprecht, V. Belagiannis, F. Tombari, and N. Navab. Deeper depth prediction with fully convolutional residual networks. *arXiv:1606.00373*, 2016.
- [17] M. Mathieu, C. Couprie, and Y. LeCun. Deep multi-scale video prediction beyond mean square error. *arXiv:1511.05440*, 2015.
- [18] V. Michalski, R. Memisevic, and K. Konda. Modeling deep temporal dependencies with recurrent grammar cells. *NIPS*, 2014.
- [19] J. Oh, X. Guo, H. Lee, R. L Lewis, and S. Singh. Action-conditional video prediction using deep networks in atari games. In *NIPS*, 2015.
- [20] M. Ranzato, A. Szlam, J. Bruna, M. Mathieu, R. Collobert, and S. Chopra. Video (language) modeling: a baseline for generative models of natural videos. *arXiv:1412.6604*, 2014.
- [21] E. Santana and G. Hertz. Learning a driving simulator. *arXiv:1608.01230*, 2016.
- [22] N. Srivastava, E. Mansimov, and R. Salakhutdinov. Unsupervised learning of video representations using lstms. *arXiv:1502.04681*, 2015.
- [23] C. Vondrick, H. Pirsiavash, and A. Torralba. Anticipating visual representations from unlabeled video. *CVPR*, 2016.
- [24] J. Walker, A. Gupta, and M. Hebert. Dense optical flow prediction from a static image. In *ICCV*, pages 2443–2451, 2015.
- [25] T. Xue, J. Wu, K. Bouman, and Freeman W. Probabilistic modeling of future frames from a single image. *NIPS*, 2016.